ADVANCED OPTICAL MATERIALS
www.advopticalmat.de

Active Control of Electromagnetically Induced Transparency Analog in Terahertz MEMS Metamaterial

*Prakash Pitchappa, Manukumara Manjappa, Chong Pei Ho, Ranjan Singh, Navab Singh, and Chengkuo Lee**

Electromagnetic metamaterials are artificially engineered materials that have revolutionized the research activities for efficient manipulation of terahertz (THz) waves in the past decade. The unprecedented advantage of metamaterial comes from its extreme scalability, as the electromagnetic properties of metamaterial are primarily determined by the unit cell geometry. This has led to the demonstration of interesting properties in THz spectral region such as artificial magnetism, negative refractive index, unnaturally large refractive index, wavelength selective absorption, chirality, and classical analog of electromagnetically induced transparency (EIT).[1–7] EIT analog demonstrated using planar metamaterials can enable interesting applications desiring slow light behavior and high nonlinearity.[8–12] EIT in metamaterial is realized through near-field coupling between the bright and dark mode resonators. The dark mode resonator with the sharp resonance is excited as radiative mode within the broader absorption spectrum of the bright mode resonator. In these coupled systems, there are three primary parameters: resonant frequency of the bright mode, resonant frequency of the dark mode, and coupling distance between them. Recently, active modulation of EIT phenomenon has been reported through dynamic modulation of the resonant frequency of dark mode resonator[13–15] or the intercoupling distance.[16] Reports on active modulation of EIT include optically controlled photoconductive materials[13–17] or thermally controlled superconducting materials as the part of coupled resonator system.[18] Tunability in coupled resonator system adds a new dimension to the functionality of these metamaterials and their possible applications. The ultimate form of active manipulation of EIT phenomenon will be when all three primary parameters are controlled independently. The independent control of individual resonators demands for the controllability at unit cell level, and conventional approaches such as optical pumping of photoconductive elements or thermally controlled superconductor are restricted to provide only global control.

Recently, microelectromechanical systems (MEMS) based tunable metamaterials have been reported to achieve controllability at unit cell level, along with the added advantage of being electrically controlled, miniaturized size and enhanced electro-optic performance. The versatility of MEMS design has enabled active manipulation of numerous THz properties such as magnetic resonance,[19–22] electrical resonance,[23–25] anisotropy,[26] broadband response,[27] isotropic resonance switching[28] multiresonance switching,[29–31] and coupling strength between resonators.[32] The enhanced controllability and direct integration of MEMS actuators into metamaterial unit cell geometry is an ideal fit for the realization of selective control of coupled mode resonators. In this Communication, reconfigurable metamaterial with independently controlled bright and dark mode resonators is proposed for advanced manipulation of the classical analog of EIT and slow light effects in THz spectral region. The active control of bright mode resonator enables modulation of EIT intensity, while the tuning of dark mode resonance causes the EIT peak to tune in frequency. Furthermore, simultaneous switching of bright and dark mode resonators results in dynamic switching of the system between coupled and uncoupled states. The proposed approach of selective reconfiguration can be scaled for multiresonator systems, which can be coupled either through inductive, capacitive, or conductive means.

The metamaterial consists of 80 × 80 periodic array of cut wire resonator (CWR) with closely placed split ring resonators (SRRs), as shown in **Figure 1** and **Figure 2**. The periodicity of unit cell is 100 µm along both axial directions. The CWR has length, l_C = 60 µm and width, w_C = 5 µm, respectively. The SRRs have a base length, b_S = 30 µm, side length, l_S = 20 µm, and split gap, g_S = 4 µm. The SRRs are placed at a distance of S = 2 µm from the CWR. When the polarization of the excitation field is along the CWR arm, the dipole mode resonance of the CWR will be the bright mode and the inductive-capacitive (LC) mode of SRR resonance acts as the dark mode. Thus for the incident THz polarization, the direct excitation of the bright mode induces image charges on the nearby SRRs through near-field inductive coupling, thereby exciting the LC resonance of the SRRs. These bright-dark resonances have contrasting line widths with identical resonance frequencies and under a strong coupling regime they experience an EIT-type of interference that gives rise to a sharp transmission peak. Thus, through

P. Pitchappa, C. P. Ho, Prof. C. Lee
Department of Electrical and Computer Engineering
National University of Singapore
Singapore 117576, Singapore
E-mail: elelc@nus.edu.sg
P. Pitchappa, C. P. Ho, Prof. C. Lee
National University of Singapore
Suzhou Research Institute
Suzhou 215123, China
M. Manjappa, Prof. R. Singh
Division of Physics and Applied Physics
Centre for Disruptive Photonic Technologies
School of Physical and Mathematical Sciences
Nanyang Technological University
Singapore 637371, Singapore
P. Pitchappa, C. P. Ho, Dr. N. Singh
Institute of Microelectronics
Agency for Science, Technology, and Research (A*STAR)
11 Science Park Road
Singapore Science Park II
Singapore 117685, Singapore

DOI: 10.1002/adom.201500676

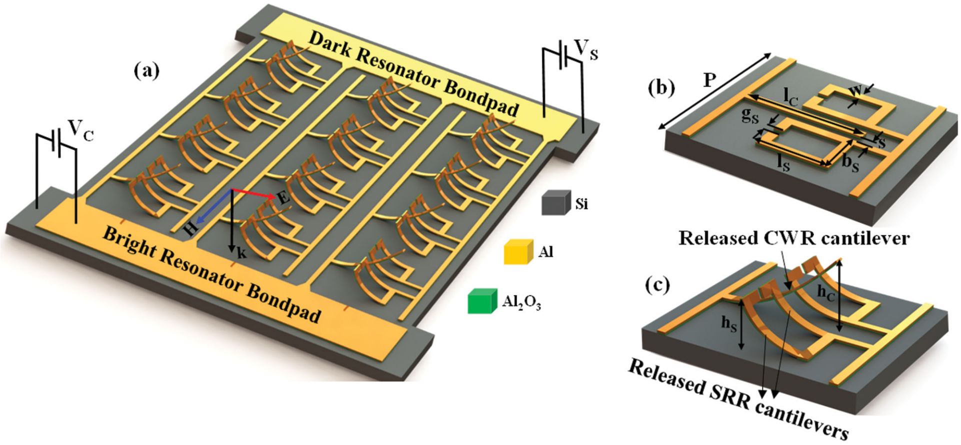

Figure 1. a) Illustrative schematics of the proposed MEMS metamaterial with independently reconfigurable CWR and SRR released microcantilevers and metamaterial unit cell with both CWR and SRR microcantilevers in b) OFF states and c) ON states, respectively, with the geometrical parameters definitions.

independent control of resonance frequencies of the bright and dark mode resonators and the intercoupling distance between them, the EIT can be actively modulated in intensity as well as tuned in frequency based on the specific on-demand functionalities.

The metamaterial is made of bimaterial layers—500 nm aluminum (Al) on top of 50 nm aluminum oxide (Al_2O_3), fabricated on top of 8 inch lightly doped silicon (Si) substrate as described next.[21,24] The bare Si wafer is cleaned and 100 nm thick thermal silicon-di-oxide (SiO_2) layer is deposited. This SiO_2 layer acts as the sacrificial layer used to release the microcantilevers. The anchor regions are defined using photolithography and SiO_2 is dry etched using reactive ion etching process. Then, 50 nm thick Al_2O_3 layer is deposited using atomic layer deposition (ALD) process, followed by 500 nm of sputter deposition of Al. At this point, the bimorph layers (Al/Al_2O_3) are in physical contact with Si at the anchor region where the SiO_2 is etched away before the bilayer deposition and on the other part of the wafer, the bilayer is on top of SiO_2 layer. Another photolithography step is used to define the metamaterial unit cell geometry, metal line, and bondpads. Both Al and Al_2O_3 are dry etched subsequently. It is important to note that the part of metamaterial unit cells that needs to be released are in top of SiO_2 layer and the other regions are anchored to Si substrate. Finally, vapor hydrofluoric acid (VHF) is used to isotropically

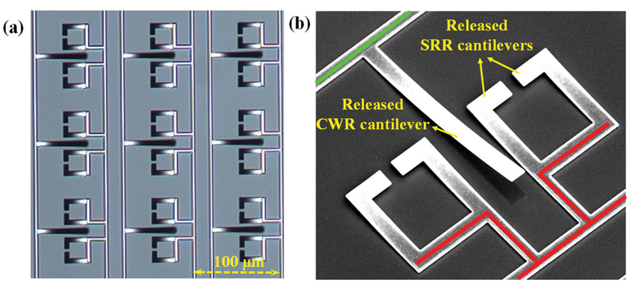

Figure 2. a) Optical microscope image of the fabricated MEMS metamaterial and b) scanning electron microscope image of fabricated unit cell of metamaterial with both CWR and SRR microcantilevers in OFF state.

remove the SiO_2 sacrificial layer from underneath the microcantilever structures, thereby suspending them over the Si substrate with an air gap. Due to the residual stress in the bimorph cantilevers, the released cantilevers are bent up, and the air gap is much higher than the thickness of sacrificial layer. Here, one end of CWR is fixed to the substrate and the CWR along the entire length is released. In case of SRRs, the base side is fixed, while the side arms along with the gap bearing tip sides are released. The released cantilevers integrated with CWR and SRRs forming the MEMS metamaterial unit cell are schematically shown in Figure 1c. The gradient of the curvature of the fabricated microcantilevers from the tip to the anchor point can be clearly seen in Figure 2. The initial tip displacement of the fabricated CWR and SRR microcantilevers is measured to be $h_C \approx 10$ µm and $h_S \approx 2.5$ µm, respectively. When voltage is applied across the Al lines of the released cantilevers and Si substrate, the cantilevers deform toward the fixed substrate due to the attractive electrostatic force. This physical deformation will introduce the restoring force, which will act in the opposite direction to the electrostatic force. Hence, at a given voltage, the final position of the cantilever is determined as the point where the electrostatic and restoring forces balance out each other. When the applied voltage increases, the electrostatic force increases much sharply than the restoring force. Hence, after a critical value of applied voltage called the "Pull-in voltage" (V_{PI}), the microcantilever will come in physical contact with the Si substrate.[33–35] Based on the applied voltage and physical position of the released cantilevers two states are defined for each resonator: "OFF" state—when no voltage is applied and air gap exists between the microcantilevers and Si substrate—and "ON" state—when the applied voltage is greater than V_{PI} and the microcantilevers are in physical contact with Si substrate. Importantly, the metal line connecting the CWRs is isolated from that of SRRs and this allows for the independent reconfiguration of bright and dark mode resonances in MEMS metamaterial. Hence, the metamaterial can be in one of the four possible configurations—CWR-ON/SRR-ON, CWR-OFF/SRR-ON, CWR-ON/SRR-OFF, and CWR-OFF/SRR-OFF (please refer to Figure S1, Supporting Information).

Conventionally, the modulation of EIT analog is achieved by controlling the resonance strength of the dark mode resonator or altering the coupling distance between the resonators. Here, a novel approach for EIT modulation is demonstrated by actively changing the strength of the bright mode resonator at a specific frequency, by tuning the resonance frequency of the broader dipole resonance of CWR, rather than modulating the LC resonance of SRRs as demonstrated in earlier reports.[13] The resonant frequency of CWR is actively controlled by changing the out-of-plane displacement of the CWR cantilever, while the SRR microcantilevers are kept fixed to the Si substrate. The physical position of released CWR and SRR microcantilevers are defined by their respective release angles, $\theta_C = \tan^{-1}(h_C/l_C)$ and $\theta_S = \tan^{-1}(h_S/S_S)$. Finite-difference time-domain (FDTD) simulations were carried out with the continuously varying θ_C from the initial state of 0° to 2°, while θ_S was kept constant at 0°. The simulated transmission spectra for the metamaterial with varying θ_C are shown in **Figure 3**a. It can be seen that when $\theta_C = 0°$ and $\theta_S = 0°$, there is a sharp transmission peak within the broader absorption spectra at 0.55 THz. This is a signature of the strong plasmonic hybridization in the system. The surface current excitation is shown in Figure 3b and there is a strong current along the CWR and circulating current in the SRRs. The induced current in CWR is same as the direction of the excitation field, hence confirms the dipolar mode resonance excitation at 0.55 THz. On the other hand, the gap bearing side of SRR is perpendicular to the polarization of the excitation field and the resulting strong circulating current is caused due to the strong inductive coupling with the bright CWR. The EIT peak has an amplitude of 0.7 at 0.55 THz for $\theta_C = 0°$. When θ_C increases, the resonant frequency of the CWR is strongly blue shifted and the amplitude of incident THz waves coupled to CWR at 0.55 THz drops significantly. This weakens the excitation of the dark mode LC resonance of SRRs at 0.55 THz. Additionally, the physical out-of-plane displacement of CWR microcantilevers could further weaken the coupling strength between the CWR and SRRs. However, the effect of increase in physical displacement should be minimal, as the distance is an order of magnitude smaller than the incident THz wavelength. As the dipolar mode resonance of the CWR is much broader than the SRR LC mode resonance, EIT peak is observed even at higher θ_C. However, the amplitude of transparency peak decreases significantly when θ_C increases as shown in Figure 3a. At $\theta_C = 2°$, there is no more observable transparency peak in the spectral region of interest. The simulated surface current at 0.63 THz in Figure 3c also shows that the resonance is directly excited in the metal interconnects in the SRRs by the incident THz waves. It can also be observed that with increasing θ_C, the entire hybridized spectrum shows a slight blue shift in the frequencies of the hybridized modes as seen in Figure 3a. According to the coupled oscillator model[12] for the plasmonic hybridization, the resonance frequency of the dark mode will be closer to the frequency of the transmission peak, whereas the bright mode resonance frequency remains closer to the symmetric mode of the coupled system. The observed blue shift in the frequencies of bright as well as the dark resonances in the coupled/hybridized system is due to the change in the coupling strength between the bright and the dark resonator as the θ_C is gradually increased. The coupling strength between the resonators dictates the frequencies of the bright and the dark modes in the hybridized system.

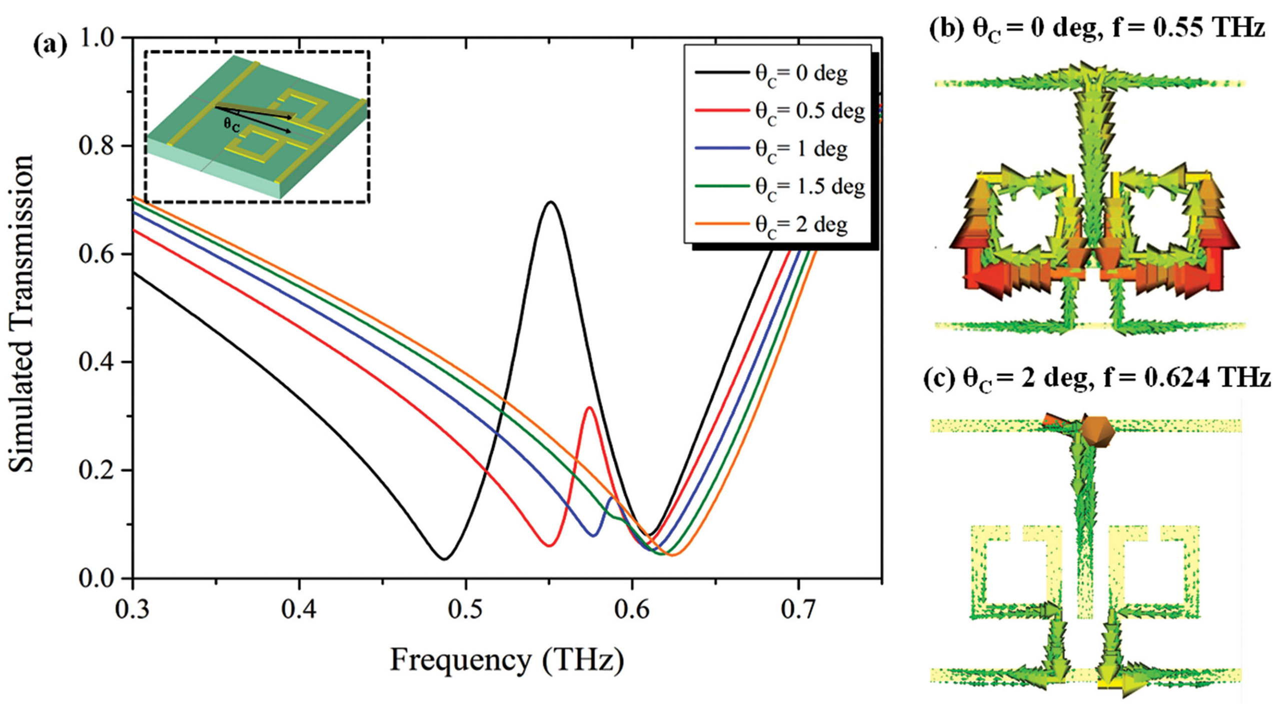

Figure 3. a) Simulated transmission spectra of MEMS metamaterial with varying θ_C from 0° to 2°, while θ_S is kept at 0°. The simulated surface current for MEMS metamaterial for b) $\theta_C = 0°$ at 0.55 THz and c) $\theta_C = 2°$ at 0.63 THz, respectively.

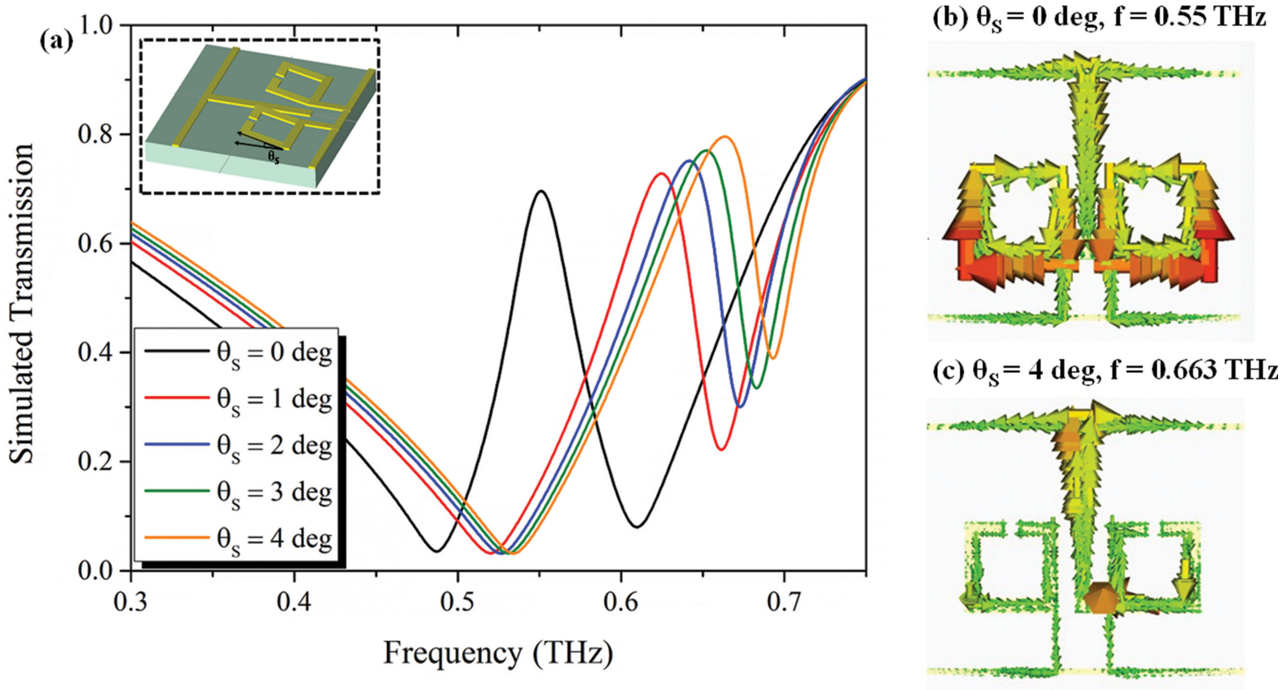

Figure 4. a) Simulated transmission spectra of MEMS metamaterial with varying θ_S from 0° to 4°, while θ_C is kept at 0°. The simulated surface current for MEMS metamaterial for b) $\theta_S = 0°$ at 0.55 THz and c) $\theta_S = 2°$ at 0.66 THz, respectively.

To study the effect of tuning the dark mode resonant frequency, θ_S was continuously varied from 0° to 4°, while keeping θ_C at 0°. The simulated transmission spectra for the metamaterial with varying θ_S are shown in **Figure 4**a. It can be observed that as θ_S increases from 0° to 4°, the EIT peak blue shifts from 0.55 to 0.66 THz. The CWR resonance is much broader than the SRR resonance and hence even when θ_S is increased, the blue shifted SRR resonant frequency falls within the wider absorption spectrum of ON state CWR dipolar resonance. Figure 4b shows the strong excitation of the radiative LC mode resonance of SRR at $\theta_S = 0°$ due to the near-field coupling with the CWR. Similarly, Figure 4c shows that at 0.663 THz, there is a weaker circulating current distribution in the SRR for $\theta_S = 4°$. Hence, the coupling between the CWR and SRR still exists, but is weakened due to mismatch in the resonant frequencies of CWR and SRR and also due to the relative difference in the physical position of the released CWR and SRR microcantilevers. It is also interesting to note that the transmission peak shows an increasing asymmetry as θ_S increases. This is quite expected, because the dipolar resonance of the CWR remains at 0.55 THz for all θ_S, while the blue shift in the SRR LC mode resonant frequency causes the EIT peak to fall at the tailing end of the dipolar resonance spectrum. Thus, active tuning of EIT resonance frequency can be achieved by controlling the SRR resonance frequency, while keeping the CWR resonance unchanged.

The fabricated metamaterial is characterized using transmission mode THz time-domain spectroscopy (THz-TDS) for different reconfiguration states by appropriately biasing the CWR and SRR cantilevers. The incoming THz wave illuminates the metamaterial at normal incidence with electric field linearly polarized along the CWR arm. For the CWR-ON/SRR-ON configuration, where both the CWR and SRR resonators are in physical contact with the substrate, the measured as well as simulated transmission responses for metamaterial in CWR-ON/SRR-ON configuration are shown in **Figure 5**a and the inset shows the OM image of the metamaterial in the corresponding state. The measured data (solid line) show good agreement with the simulated curve (dotted-line). In this case, the individual resonances, dipolar resonance of CWR (bright mode) and LC mode resonance of SRR (dark mode) fall at the same resonance frequency but possess contrasting line widths. The LC mode resonance of SRR is excited by the virtue of near-field coupling to the bright mode and gives rise to a sharp transmission peak (please refer to Figure S2, Supporting Information). This mechanism is purely based on the classical analog of EIT interference effect, where the two resonators possessing contrasting decay rates at identical resonance frequencies interfere destructively giving rise to a sharp transmission peak at the resonance.[6] The transmission spectrum for the CWR-OFF/SRR-ON state is shown in Figure 5b. This system displays two transmission windows: one being sharp yet weak transmission peak centered at 0.65 THz and the other being the broad transmission window centered at 0.8 THz. Evolution of the sharp transmission peak at 0.65 THz is due to the excitation of the dark mode LC resonance of primary SRR through simultaneous inductive coupling of the nearby CWR dipole mode along with the conductively coupled bright mode LC resonance of the secondary SRR, which is formed by the base of primary SRR and the metal interconnects (see the Supporting Information).[7] The second transparency window centered at 0.8 THz is due to the interaction between the bright mode, i.e., dipolar

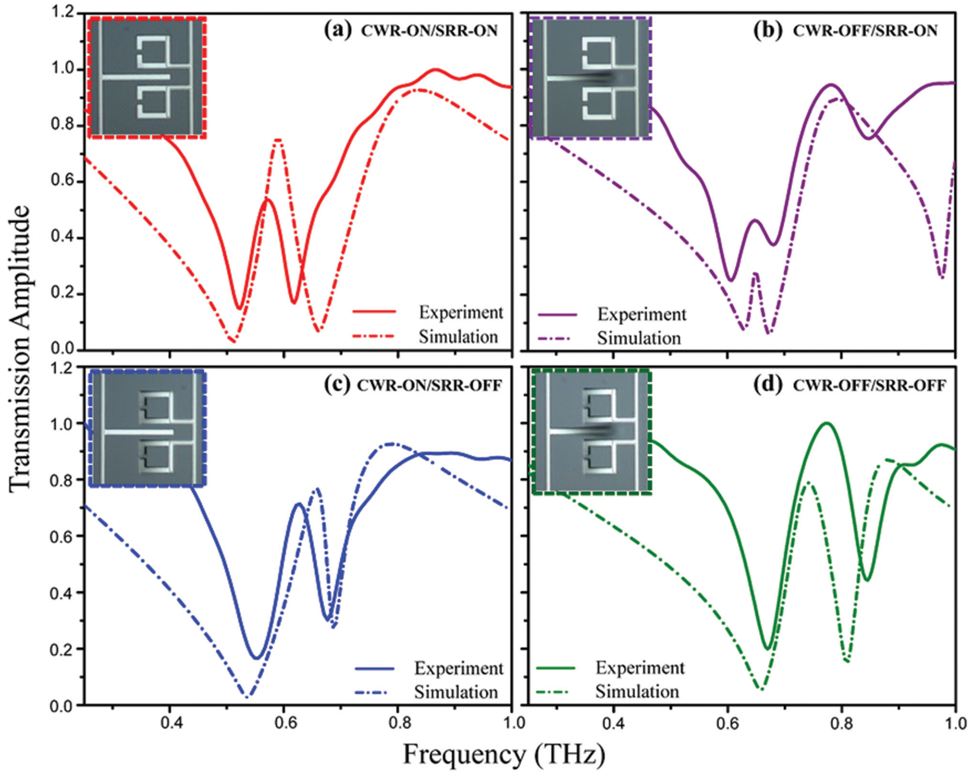

Figure 5. Measured and simulated THz transmission response of the MEMS metamaterial in a) CWR-ON/SRR-ON, b) CWR-OFF/SRR-ON, c) CWR-ON/SRR-OFF, and d) CWR-OFF/SRR-OFF states. The insets show the OM image of the fabricated MEMS metamaterial in the respective states. The OFF state can be seen as the gradually varying focus along the length of the cantilever, while in the ON state the entire cantilever is in focus as it is in physical contact with Si substrate.

mode of CWR in OFF state and the bright LC mode of the secondary SRR structure in ON state. This leads to broader transmission window due to the hybridization of the bright modes. For the case of CWR-ON/SRR-OFF configuration, a Fano-type of interference between the bright dipolar mode of CWR and LC mode dark resonance of primary SRR appears and results in the observed asymmetric nature of transmission. The comprehensive study on the coupling schemes in these structures is detailed in Figure S4 of the Supporting Information.[36] Besides the independent control of bright and dark mode resonators to actively tune the transparency in the system, both the individual resonators can be simultaneously actuated to completely change the system from the strongly coupled to uncoupled configuration or vice versa. Figure 5d shows the transmission response of the coupled system under the simultaneous reconfiguration of CWR and SRR to OFF state. In the OFF states, the individual resonances of the dark SRR and bright CWR appear far apart that weakens the bright-dark coupling and results in the asymmetric nature of the transmission. The nature of the coupling can be well described by the nature of the induced surface currents within the resonators and is detailed in Figure S5 of the Supporting Information. The enhanced controllability in MEMS metamaterial enables the active tuning of the coupling between resonators to switch from strong, moderate, weak to even uncoupled configuration.

The active modulation of the transmission properties of the coupled system is utilized to demonstrate the dynamic control of the slow light behavior in the proposed metamaterial. **Figure 6** shows experimentally measured group delay of the THz pulses propagating through the MEMS metamaterial sample in different reconfiguration states, which depict the degree of slow light behavior in the system. The group delay for the pulses is given by $t_g = -d\phi/d\omega$, where ϕ is the phase and ω is the angular frequency of the THz pulse. The delay band width product (DBP) is defined as the product of maximum group delay and the spectrum bandwidth (DBP = $t_g \times \Delta f$). DBP is a figure of merit to determine the efficiency of the devices for telecommunication channels, where the maximum DBP implies that the device is more efficient to store and transmit the information through the signal channel. The calculated DBP for the fabricated MEMS metamaterial is listed in **Table 1** along with the respective value of the group delay. The measured DBP for the metamaterial in CWR-ON/SRR-OFF state has the larger value of 0.32 at 0.55 THz, whereas in CWR-OFF/SRR-ON state it has the smallest value of 0.04 at 0.65 THz. Thus, the proposed metamaterial allows for active modulation of DBP up to an order of magnitude by dynamic control of the transmission properties by using the MEMS design, which would enhance the use of MEMS based metamaterials devices in the future THz telecommunication networks.

In summary, the proposed MEMS metamaterial enables the independent reconfiguration of near-field coupled bright and dark mode resonators for active modulation and frequency tuning of the EIT analog in terahertz spectral region. Simul-

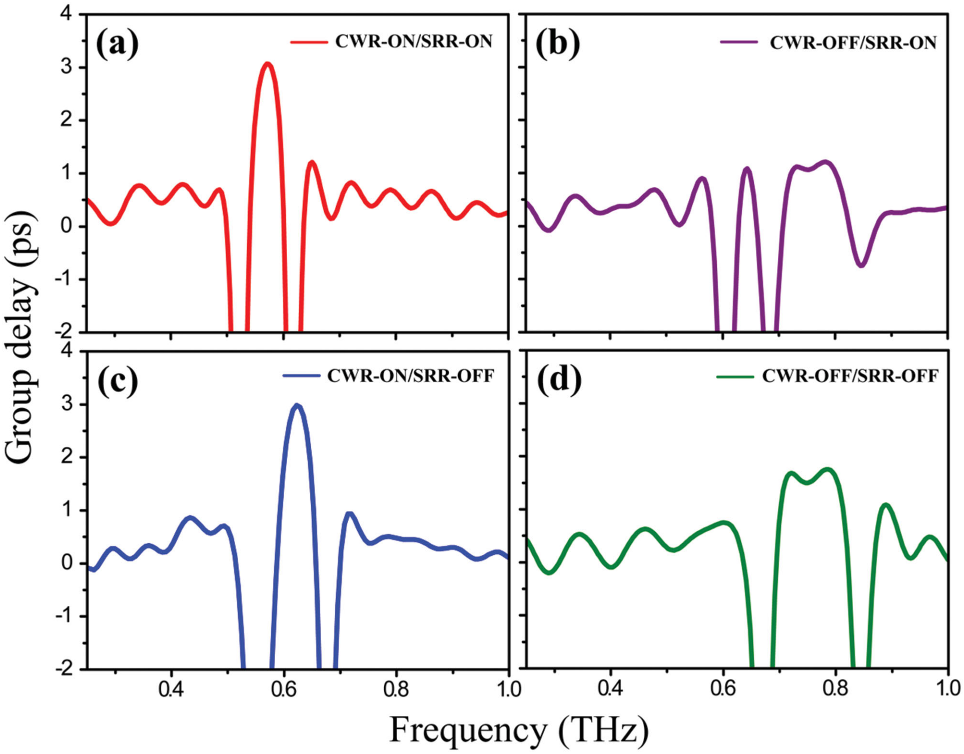

Figure 6. Measured THz group delay for the MEMS metamaterial in a) CWR-ON/SRR-ON, b) CWR-OFF/SRR-ON, c) CWR-ON/SRR-OFF, and d) CWR-OFF/SRR-OFF configuration states, respectively.

taneous reconfiguration of bright and dark mode resonators enables the dynamic switching of the system from coupled to uncoupled mode and vice versa. These metamaterials provide electrically controlled group delay of the THz waves that are attractive for THz optical delay lines and buffer devices. Furthermore, dynamically reconfiguring the channel capacity of the proposed metamaterial will be critical for the next-generation-high-speed sub-THz wireless communication systems. These metamaterials are electrically controlled, highly miniaturized, and are fabricated using complementary metal-oxide-semiconductor (CMOS) compatible materials and processes, hence making them the perfect choice for the realization of THz slow light and high performance nonlinear devices. The versatility of microactuators along with ease of integration into metamaterial geometry with enhanced controllability allows for more exciting works in the field of coupled resonator system for both in-plane and out-of-plane coupled systems.

Table 1. Experimentally obtained group delay and delay bandwidth product (DBP) for selectively reconfigurable coupled-mode resonators THz MEMS metamaterial.

Reconfiguration state of MEMS metamaterial	Group delay [ps]	Delay bandwidth product (DBP)
CWR-ON/SRR-ON	3.07	0.18
CWR-OFF/SRR-ON	1.09	0.04
CWR-ON/SRR-OFF	2.98	0.32
CWR-OFF/SRR-OFF	1.5	0.28

Experimental Section

Electromagnetic Simulation: FDTD numerical simulations were conducted to calculate the transmission spectra and the electromagnetic field and surface current distributions corresponding to the resonance modes with normally incident THz waves of either TE (electric field along the CWR arm) or TM (along the gap bearing side of SRR) polarization. Full-field electromagnetic wave simulations were performed using the commercial simulation software Computer Software Technology (CST) Microwave studio 2009. For the material property, Aluminum was modeled as lossy metal with conductivity of 1e7 S m^{-1}. Aluminum oxide and silicon were modeled as lossless dielectric with dielectric constant of 9.5 and 11.9, respectively. In the simulation, a single unit cell of the metamaterial structures was simulated with unit cell boundary conditions employed in axial directions orthogonal to the incident waves. The perfectly matched layers were applied along the propagation of the electromagnetic waves. Plane waves were incident into the unit cell from the port on the metal side, while the transmission spectrum was determined from the port placed at the other side of metamaterial. In the meanwhile, field monitors were used to collect the electric fields, magnetic fields, and the respective surface currents at different resonance frequencies.[28, 31]

Electromechanical Characterization: The deflection profile of released microcantilevers for CWR and SRR was measured using Lyncee Tec. reflection digital holographic microscope (R-DHM). The released chips were wire bonded to a printed circuit board (PCB). One voltage power supply for actuating the CWR cantilevers and other for SRR cantilevers were used, respectively. Si substrate was kept at ground potential, and the microcantilevers were positively biased. The voltage was increased between the microcantilevers and Si substrate and when the applied voltage was higher than the pull in voltage, the microcantilevers came in physical contact with the Si substrate.[25,28,31] The Al_2O_3 layer beneath the Al layer ensured that there was no current flowing from Al layer to Si substrate, when pull in occurred. This is crucial because if the current flows through the Al/Si junction, then the temperature will raise up locally, thereby melting the Al tips with the Si substrate, and will permanently damage the device. At different applied voltage, the cantilever profile can be measured directly from the R-DHM unit. The electrical isolation between the CWR and SRR allows for independent reconfiguration of CWR and SRR microcantilevers.

Terahertz Transmission Measurement: The THz transmission spectra characterization was measured using Teraview 3000 time-domain spectroscopy (THz-TDS) system. The THz waves were incident normally with electric field along the length of the CWR arm. The wire bonded chip was then applied with desired voltage from an externally connected dual source Agilent E3646A power supply—one for CWR and other for SRR. When the applied voltage is 0 V, the cantilevers are in OFF state, 30 V is applied to switch the CWR, and SRR cantilevers to ON state. When the voltage was brought back to 0 V, the cantilevers came back to the original OFF state.[23–25,28,31] The transmission spectra were then measured for the MEMS metamaterial in both ON and OFF states. The transmission spectra were normalized with respect to transmission of pure silicon substrate of the same thickness as the samples.

Acknowledgements

The authors acknowledge the financial support from research grant of AcRF Tier 2-MOE2012-T2-2-154 at the National University of Singapore and the National Natural Science Foundation of China (Grant No. 61474078) at the National University of Singapore Suzhou Research Institute (NUSRI), Suzhou, China.

Received: November 17, 2015
Revised: December 15, 2015
Published online: January 12, 2016

[1] T. J. Yen, W. J. Padilla, N. Fang, D. C. Vier, D. R. Smith, J. B. Pendry, D. N. Basov, X. Zhang, *Science* **2004**, *303*, 5663.
[2] M. Gokkavas, K. Guven, I. Bulu, K. Aydin, R. S. Penciu, M. Kafesaki, C. M. Soukoulis, E. Ozbay, *Phys. Rev. B* **2006**, *73*, 193103.
[3] M. Choi, S. H. Lee, Y. Kim, S. B. Kang, J. Shin, M. H. Kwak, K. Y. Kang, Y. H. Lee, N. Park, B. Min, *Nature* **2011**, *470*, 7334.
[4] H. Tao, N. I. Landy, C. M. Bingham, X. Zhang, R. D. Averitt, W. J. Padilla, *Opt. Express* **2008**, *16*, 10.
[5] E. Plum, J. Zhou, J. Dong, V. A. Fedotov, T. Koschny, C. M. Soukoulis, N. I. Zheludev, *Phys. Rev. B* **2009**, *79*, 035407.
[6] S. Y. Chiam, R. Singh, C. Rockstuhl, F. Lederer, W. Zhang, A. A. Bettiol, *Phys. Rev. B* **2009**, *80*, 153103.
[7] R. Singh, C. Rockstuhl, F. Lederer, W. Zhang, *Phys. Rev. B* **2009**, *79*, 085111.
[8] N. Papasimakis, V. A. Fedotov, N. I. Zheludev, *Phys. Rev. Lett.* **2008**, *101*, 253903.
[9] P. Tassin, L. Zhang, T. Koschny, E. N. Economou, C. M. Soukoulis, *Opt. Express* **2009**, *17*, 7.
[10] N. Liu, L. Langguth, T. Weiss, J. Kästel, M. Fleischhauer, T. Pfau, H. Giessen, *Nat. Mater.* **2009**, *8*, 9.
[11] Y. Yang, I. I. Kravchenko, D. P. Briggs, J. Valentine, *Nat. Commun.* **2014**, *5*, 5753.
[12] M. Manjappa, S. Y. Chiam, L. Cong, A. A. Bettiol, W. Zhang, R. Singh, *Appl. Phys. Lett.* **2015**, *106*, 181101.
[13] J. Gu, R. Singh, X. Liu, X. Zhang, Y. Ma, S. Zhang, S. A. Maier, Z. Tian, A. K. Azad, H. T. Chen, A. J. Taylor, J. Han, W. Zhang, *Nat. Commun.* **2012**, *3*, 1151.
[14] D. R. Chowdhury, R. Singh, A. J. Taylor, H. T. Chen, A. K. Azad, *Appl. Phys. Lett.* **2013**, *102*, 011122.
[15] F. Miyamaru, H. Morita, Y. Nishiyama, T. Nishida, T. Nakanishi, M. Kitano, M. W. Takeda, *Sci. Rep.* **2014**, *4*, 4346.
[16] X. Su, C. Ouyang, N. Xu, S. Tan, J. Gu, Z. Tian, R. Singh, S. Zhang, F. Yan, J. Han, W. Zhang, *Sci. Rep.* **2015**, *5*, 10823.
[17] Y. Bai, K. Chen, H. Liu, T. Bu, B. Cai, Jian Xu, Y. Zhu, *Opt. Commun.* **2015**, *353*, 83.
[18] W. Cao, R. Singh, C. Zhang, J. Han, M. Tonouchi, W. Zhang, *Appl. Phys. Lett.* **2013**, *103*, 101106.
[19] H. Tao, A. C. Strikwerda, K. Fan, W. J. Padilla, X. Zhang, R. Averitt, *Phys. Rev. Lett.* **2009**, *103*, 147401.
[20] W. M. Zhu, A. Q. Liu, X. M. Zhang, D. Ping Tsai, T. Bourouina, J. H. Teng, X. H. Zhang, H. C. Guo, H. Tanoto, T. Mei, G. Q. Lo, D. L. Kwong, *Adv. Mater.* **2011**, *23*, 15.
[21] Y. S. Lin, Y. Qian, F. Ma, Z. Liu, P. Kropelnicki, C. Lee, *Appl. Phys. Lett.* **2013**, *102*, 11.
[22] Z. Han, K. Kohno, H. Fujita, K. Hirakawa, H. Toshiyoshi, *Opt. Express* **2014**, *22*, 18.
[23] F. Ma, Y. Qian, Y. S. Lin, H. Liu, X. H. Zhang, Z. Liu, J. M. L. Tsai, C. Lee, *Appl. Phys. Lett.* **2012**, *102*, 16.
[24] F. Ma, Y. S. Lin, X. H. Zhang, C. Lee, *Light: Sci. Appl.* **2014**, *3*, e171.
[25] P. Pitchappa, C. P. Ho, L. Dhakar, Y. Qian, N. Singh, C. Lee, *J. Microelectromech. Syst.* **2015**, *24*, 3.
[26] W. M. Zhu, A. Q. Liu, T. Bourouina, D. P. Tsai, J. H. Teng, X. H. Zhang, G. Q. Lo, D. L. Kwong, N. I. Zheludev, *Nat. Commun.* **2012**, *3*, 1274.
[27] M. Unlu, M. R. Hashemi, C. W. Berry, S. Li, S. H. Yang, M. Jarrahi, *Sci. Rep.* **2014**, *4*, 5708.
[28] P. Pitchappa, C. P. Ho, Y. Qian, L. Dhakar, N. Singh, C. Lee, *Sci. Rep.* **2015**, *5*, 11678.
[29] A. Lalas, N. Kantartzis, T. Tsiboukis, *Europhys. Lett.* **2014**, *107*, 58004.
[30] C. P. Ho, P. Pitchappa, Y. S. Lin, C. Y. Huang, P. Kropelnicki, C. Lee, *Appl. Phys. Lett.* **2014**, *104*, 16.
[31] P. Pitchappa, C. P. Ho, L. Dhakar, C. Lee, *Optica* **2015**, *2*, 6.
[32] X. J. He, Q. X. Ma, P. Jia, L. Wang, T. Y. Li, F. M. Wu, J. X. Jiang, *Integr. Ferroelectr.* **2015**, *161*, 1.
[33] Y. Qian, L. Lou, J. M. L. Tsai, C. Lee, *Appl. Phys. Lett.* **2012**, *100*, 113102.
[34] P. Singh, C. G. Li, P. Pitchappa, C. Lee, *IEEE Electron Device Lett.* **2013**, *34*, 8.
[35] B. W. Soon, E. J. Ng, V. A. Hong, Y. Yang, C. H. Ahn, Y. Qian, T. W. Kenny, C. Lee, *J. Microelectromech. Syst.* **2014**, *23*, 5.
[36] R. Singh, I. A. I. Al-Naib, Y. Yang, D. R. Chowdhury, W. Cao, C. Rockstuhl, T. Ozaki, R. Morandotti, W. Zhang, *Appl. Phys. Lett.* **2011**, *99*, 201107.